ISSN 0022-4766, Journal of Structural Chemistry, 2020, Vol. 61, No. 11, pp. 1721-1728. © Pleiades Publishing, Ltd., 2020.
Russian Text © The Author(s), 2020, published in Zhurnal Strukturnoi Khimii, 2020, Vol. 61, No. 11, pp. 1817-1824.

INFLUENCE OF COMPOSITION AND CRYSTALLITE SIZE ON THERMOELECTRIC PROPERTIES OF LAYERED TUNGSTEN DICHALCOGENIDES

G. E. Yakovleva[1]*, A. Yu. Ledneva[1], A. I. Romanenko[1], V. E. Fedorov[1], B. A. Kolesov[1], and K. R. Zhdanov[1]

A series of substitutional solid solutions $W_{0.98}Nb_{0.02}Se_{2-y}Te_y$ (y = 0.2, 0.3, 0.4, 0.5) is synthesized and characterized, crystal lattice parameters are refined for phases of different composition. It is shown that the thermoelectric power of substitutional solid solutions based on modified tungsten diselenide $W_{0.98}Nb_{0.02}Se_{2-y}Q_y$ (y = 0.2, 0.3, 0.4, 0.5; Q = Te, S) depends on the substitutions in the anionic sublattice. The substitution of selenium by tellurium or sulfur in tungsten diselenide leads to an increase in the crystallite sizes. The more substituted atoms in number, the larger the crystallites, both for sulfur and tellurium cases. As the concentration of sulfur or tellurium increases, electrical conductivity and the Seebeck coefficient increase non-monotonically so that the power factor PF increases in substitutional solid solutions. Among the samples of the studied series, compound $W_{0.98}Nb_{0.02}Se_{1.5}Te_{0.5}$ has the highest PF value of 444.4 μW/m·K^2.

DOI: 10.1134/S0022476620110062

Keywords: layered transition metal dichalcogenides, crystallite sizes, electrical conductivity, Seebeck coefficient, thermoelectric power factor.

INTRODUCTION

Thermoelectricity, a phenomenon based on the Seebeck effect, is particularly interesting due to the fact that heat is directly converted into electricity. Since thermoelectric generators can use almost any heat sources, their applicability scope is expanded significantly. However, the effectiveness of such devices is limited by the effectiveness of the employed thermoelectric material. The latter is characterized by two parameters determining its capability to convert thermal energy into electrical energy: thermoelectric power factor $PF = S^2\sigma$ and dimensionless figure of merit $ZT = S^2\sigma T/k$, where S is the Seebeck coefficient; σ is electrical conductivity; k is thermal conductivity; T is temperature.

Thermoelectric properties of single-crystal samples differ notably from those of polycrystalline materials. In polycrystalline bulk materials, grain orientation and interfacial microstructure are important [1]. A reduction in grain size produces more grain boundaries, which in turn act as effective scattering centers both for the phonons and for the charge carriers. Thus, the mean free path also depends on the grain size. For example, it was established in [2] that the properties of a polycrystalline sample prepared from single crystal $Sn_{0.97}Na_{0.03}Se$ differ from those of the initial single crystal. It was shown that this discrepancy is due to the fact that partial oxidation of the powder during or after the synthesis decreases the

[1]Nikolaev Institute of Inorganic Chemistry, Siberian Branch, Russian Academy of Sciences, Novosibirsk, Russia; *galina.yakovleva.91@mail.ru. Original article submitted May 20, 2020; revised May 30, 2020; accepted June 1, 2020.

mobility of charge carriers due to the appearance of boundaries between oxidized and amorphous grains. As a result, the electrical conductivity of the polycrystal decreased by orders of magnitude in comparison with single crystals.

Currently, there is no uniform theoretical model that would relate thermoelectric properties of polycrystalline materials to crystallite sizes. The parameters of each specific compound are changed in different ways upon the variation of grain sizes of the polycrystalline material.

Among all thermoelectrics, layered compounds with strong anisotropic properties take a special place. One such widely known system is bismuth telluride Bi_2Te_3, which is most commonly used in thermoelectric generators [3]. It was shown in [4] that electrical conductivity and the Seebeck coefficient in polycrystalline films Bi_2Te_3 increase together with film thicknesses and grain sizes. In [5] it was established that reducing grain size in $Bi_{0.5}Sb_{1.5}Te_3$ alloys enhances the thermoelectric efficiency of the latter through selective suppression of bipolar conduction (decreasing the minority charge carrier mobility) and reduction of phonon conductivity due to increased scattering of low-frequency phonons. In a layered sample $Bi_{86.5}Sb_{13.5}$, electrical conductivity and the Seebeck coefficient increased with increasing grain size [6]. Thus, varying grain sizes is a valid approach to control electronic and thermal properties of materials.

The present study considers a series of solid solutions based on tungsten diselenide WSe_2, which is closely related to MoS_2, a typical representative of layered transition metal dichalcogenides (TMDs) (Fig. 1). In the TMD structure, the atoms inside a layer are connected by strong covalent bonds, while the layers interact with each other through weak van der Waals forces between chalcogen atoms [7-10]. Such sort of interatomic bonds results in a pronounced anisotropy of physical properties.

Degenerate semiconductors are most appropriate for thermoelectric applications, since their electron transport properties can be varied by changing the structure of their bands. It was shown in our previous works that WSe_2 becomes a degenerate semiconductor when 2% of tungsten atoms are replaced by niobium atoms [11, 12]. Using substitutions in the anionic sublattice (Se replacement by S or by Te) in tungsten diselenide allows changing the crystallite sizes to enhance the thermoelectric power factor *PF* of these compounds.

This work reports synthesis, characterization, and a study of electrical conductivity and the Seebeck coefficient in substitutional solid solutions $W_{0.98}Nb_{0.02}Se_{2-y}Te_y$ (y = 0.2, 0.3, 0.4, 0.5). The results obtained for the series $W_{0.98}Nb_{0.02}Se_{2-y}Q_y$ (y = 0.2, 0.3, 0.4, 0.5; Q = Te, S) were subjected to comparative analysis, depending on the crystallite size and the sample composition.

EXPERIMENTAL

Substitutional solid solutions $W_{0.98}Nb_{0.02}Se_{2-y}Te_y$ (y = 0.2, 0.3, 0.4, 0.5) were prepared by the high-temperature ampoule method according to the following procedure. A stoichiometric mixture of commercially available tungsten, niobium, selenium, and tellurium powders with a total weight of 10 g were thoroughly ground and placed in a 15 mL quartz ampoule, which was then evacuated and sealed. The first heating was carried out in the following mode: heating up to 300 °C for 6 h, aging at 300 °C for 20 h, heating up to 800 °C, aging at 800 °C for 80 h, and cooling within the oven to room temperature. After the first heating, the ampoules were shaken thoroughly to homogenize the product. The second heating to 850 °C was conducted in the course of 9 hours, then the ampoules were maintained at 850 °C for 96 h and cooled down within the oven.

The X-ray powder diffraction (XRPD) of synthesized products was conducted on a Philips PW 1830/1710 automated powder diffractometer (CuK_α, graphite monochromator). Recording mode: from 5° to 70°, step 0.05°, exposure time 3 s.

To determine the chemical composition of obtained samples, a 150 mg sample was pressed under 2000 MPa and the obtained pellet was analyzed by energy dispersive X-ray analysis (EDX) on a TM3000 instrument (Hitachi).

The thermoelectric properties were measured as follows. Experimental samples were prepared by pressing the synthesized powders under 2000 MPa at room temperature. Then 2×2×10 mm samples were cut out from the pressed pellets. The thermoelectric properties of studied compounds exhibited strong anisotropy. All measurements were carried out along

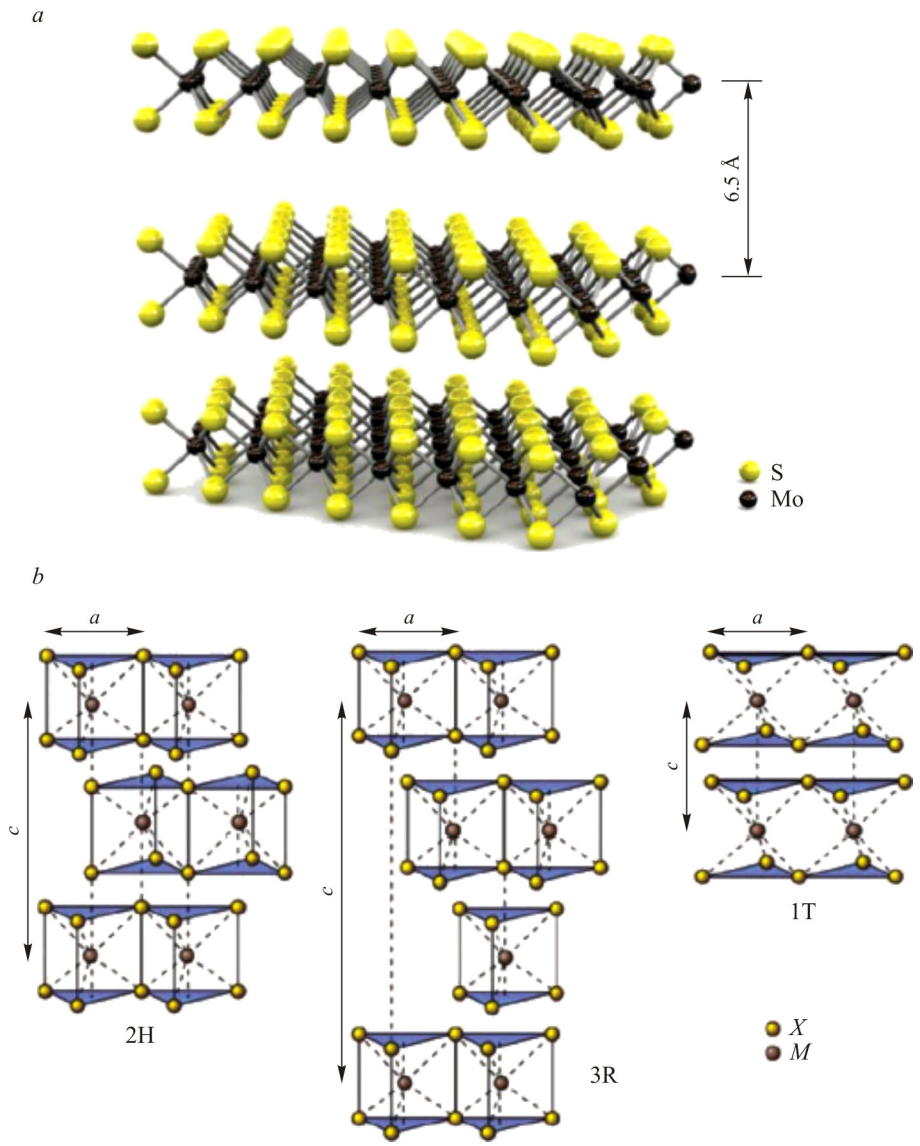

Fig. 1. Modifications of molybdenum disulfide (2H, 3*R,* and 1T).

the normal to the axis of pressing. The electrical conductivity σ was measured by the DC four-point probe method. The Seebeck coefficient *S* was measured using a variable-gradient differential method. All measurements were carried out in a helium atmosphere at room temperature. The homemade setups were developed in the Nikolaev Institute of Inorganic Chemistry.

RESULTS AND DISCUSSION

Characterization of substitutional solid solutions. The powder diffraction patterns (Fig. 2) demonstrate slightly shifted reflections corresponding to the 2H–WSe_2 phase crystallized in the $P6_3/mmc$ space group. No other WSe_2 modifications or other crystal phases were observed. Tungsten atoms form a closed-packed hexagonal layer. Each layer is surrounded by two adjacent closed-packed chalcogen layers so that the chalcogen atoms form a trigonal-prismatic environment.

The Table 1 lists refined lattice parameters and compositions according to the EDX data. Fig. 3 shows the lattice parameter *a* plotted as a function of the number of selenium atoms substituted by sulfur or tellurium in a series of compounds with general formulas $W_{0.98}Nb_{0.02}Se_{2-y}S_y$ [12] and $W_{0.98}Nb_{0.02}Se_{2-y}Te_y$. In the $W_{0.98}Nb_{0.02}Se_{2-y}S_y$ series, parameter *a* decreases

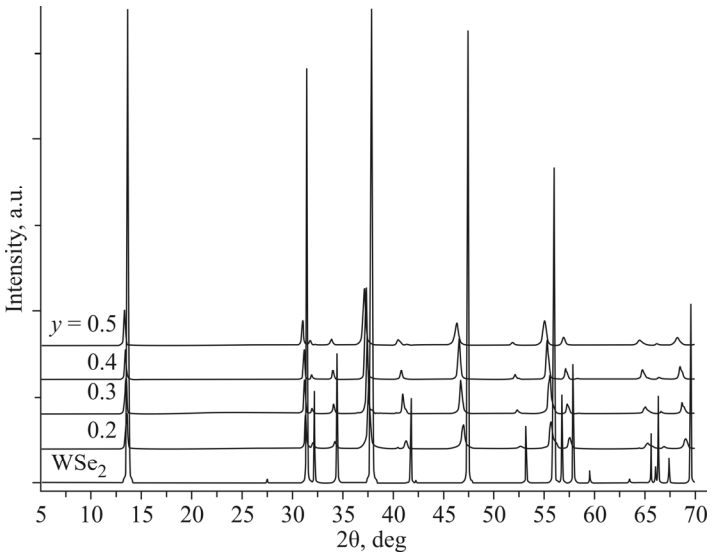

Fig. 2. Powder diffraction patterns of the $W_{0.98}Nb_{0.02}Se_{2-y}Te_y$ series (y = 0.2, 0.3, 0.4, 0.5) juxtaposed with calculated WSe_2 patterns.

TABLE 1. Refined Unit Cell Parameters in Substitutional Solid Solutions $W_{0.98}Nb_{0.02}Se_{2-y}S_y$ and $W_{0.98}Nb_{0.02}Se_{2-y}Te_y$

Formula	EDX	Refined parameter *a,* Å	Refined parameter *c,* Å
$W_{0.98}Nb_{0.02}Se_{1.8}Te_{0.2}$	$W_{0.977}Nb_{0.015}Se_{1.79}Te_{0.20}$	3.3054(16)	13.1581(31)
$W_{0.98}Nb_{0.02}Se_{1.7}Te_{0.3}$	$W_{0.98}Nb_{0.02}Se_{1.72}Te_{0.27}$	3.3121(21)	13.2073(17)
$W_{0.98}Nb_{0.02}Se_{1.6}Te_{0.4}$	$W_{0.98}Nb_{0.019}Se_{1.56}Te_{0.43}$	3.3271(18)	13.2741(36)
$W_{0.98}Nb_{0.02}Se_{1.5}Te_{0.5}$	$W_{0.98}Nb_{0.015}Se_{1.49}Te_{0.51}$	3.3394(23)	13.2894(34)
$W_{0.98}Nb_{0.02}Se_{1.8}S_{0.2}$ [12]	–	3.271	–
$W_{0.98}Nb_{0.02}Se_{1.7}S_{0.3}$ [12]	–	3.272	–
$W_{0.98}Nb_{0.02}Se_{1.6}S_{0.4}$ [12]	–	3.262	–
$W_{0.98}Nb_{0.02}Se_{1.5}S_{0.5}$ [12]	–	3.256	–
WS_2 (ICSD 202366)	–	3.153(4)	12.323(5)
WSe_2 (ICSD 40752)	–	3.282(1)	12.96(1)
WTe_2 (ICSD 73323)	–	3.477(2)	14.018(9)

as the amount of sulfur increases, while the metal–chalcogen distance decreases from 2.526 Å in WSe_2 to 2.405 Å in WS_2 (Fig. 3*a*). As the number of selenium atoms substituted by tellurium atoms increases in the $W_{0.98}Nb_{0.02}Se_{2-y}Te_y$ series, lattice parameters *a* and *c* increase almost linearly according to Vegard's law (Fig. 3*b* and *c*) in parallel with the increasing tungsten–chalcogen distance (W–Te 2.698-2.798 Å). The changes observed in the lattice parameters of obtained samples indicate the formation of substitutional solid solutions.

Fig. 4 shows the Raman spectra of $W_{0.98}Nb_{0.02}Se_{2-y}S_y$ (Fig. 4*a*) and $W_{0.98}Nb_{0.02}Se_{2-y}Te_y$ (Fig. 4*b*) compounds in comparison with the WSe_2 spectra. In the Raman spectrum of tungsten diselenide, the main vibrational bands at 247, 250, and 257 correspond to E^1_{2g}, A^1_g, and 2LA; other multiphonon modes are also present [13]. As a result of selenium atoms substitution by sulfur atoms, the peaks are redshifted, while modes E^1_{2g}, A^1_g, and E^1_{2g}–LA, A^1_g–LA are broadened similarly to $WS_{2x}Se_{2-2x}$ [14]. When selenium atoms are substituted by tellurium atoms, the intensities of modes W–Se (E^1_{2g} (W–Se) and A^1_g (W–Se) gradually decrease as the molar fraction of Te increases. Also, E^1_g (W–Se) and A^1_g (W–Se) are redshifted and are split as the molar fraction of Te decreases, similarly to the case of $WSe_{2(1-x)}Te_{2x}$ [15, 16].

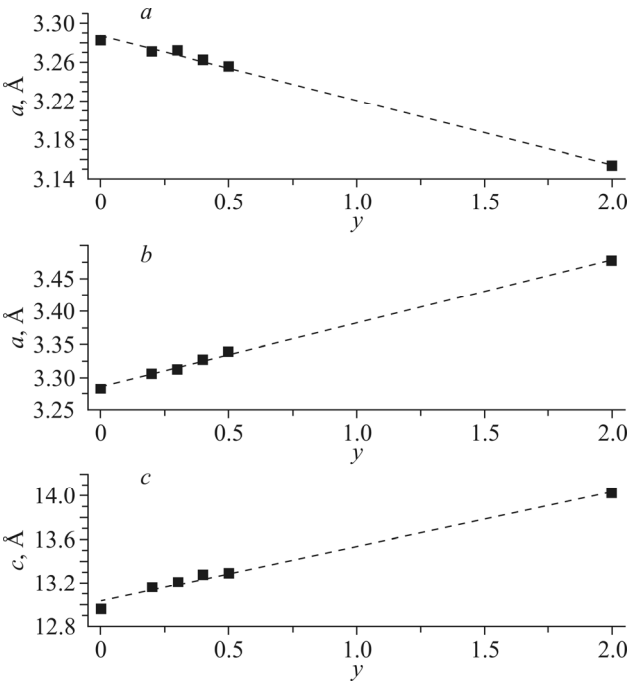

Fig. 3. Lattice parameter *a* as a function of the substituting element content in the anionic sublattice: S (*a*), Te (*b*), lattice parameter *c* as a function of Te content in the $W_{0.98}Nb_{0.02}Se_{2-y}Te_y$ series (*c*).

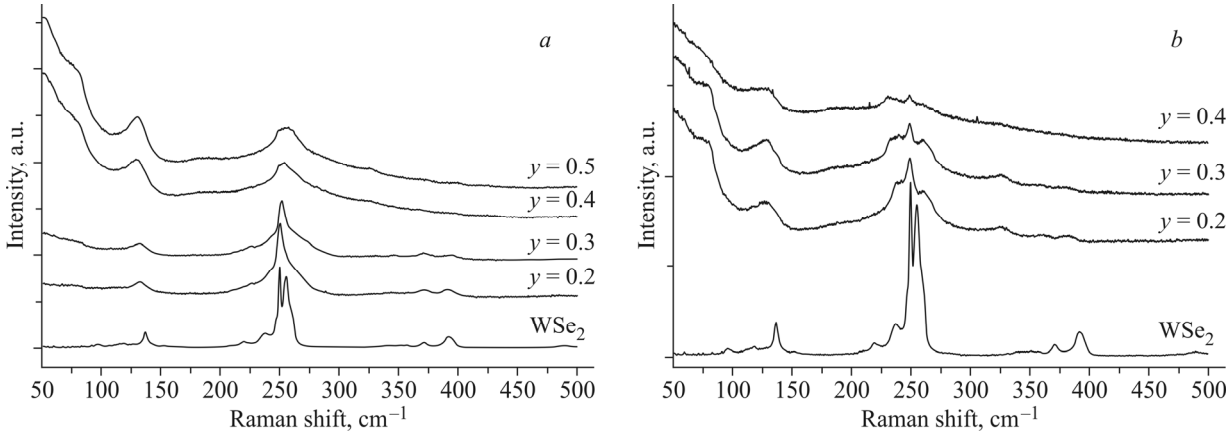

Fig. 4. Raman spectra of $W_{0.98}Nb_{0.02}Se_{2-y}Q_y$ compounds in comparison with those of WSe_2 (633 nm laser): $W_{0.98}Nb_{0.02}Se_{2-y}S_y$ (*a*), $W_{0.98}Nb_{0.02}Se_{2-y}Te_y$ (*b*).

Thermoelectric properties. Tungsten diselenide is a *p*-type semiconductor with a ~1.2 eV bandgap. Being a typical semiconductor, this material demonstrates high resistivity and a high Seebeck coefficient. Electronic transport properties can be optimized by varying the concentration of the substituting element in the cationic sublattice. Thus, it was shown in our earlier works that compound $W_{0.98}Nb_{0.02}Se_2$ has the optimal element ratio in terms of highest thermoelectric efficiency [11, 12, 17, 18]. Substitutions in the anionic sublattice have little effect on the concentration of charge carriers. However, their influence on electronic transport properties can be explained by the fact that the mobility of charge carriers is changed together with the change of crystallite sizes in polycrystalline samples. The crystallite sizes in pure WSe_2 do not exceed 3 μm. The crystallite size increases together with the concentration of the substituting element in the anionic sublattice. For

example, in the series of $W_{0.98}Nb_{0.02}Se_{2-y}S_y$ compounds, the crystallite sizes reach 7 μm for $y = 0.2$ (Fig. 5*a*) and exceed 10 μm for $y = 0.4$ (Fig. 5*b*). The same tendency is observed in the series of substitutional solid solutions $W_{0.98}Nb_{0.02}Se_{2-y}Te_y$: the crystallite sizes reach ~ 5 μm for y = 0.2 (Fig. 5*c*) and exceed 10 μm for $y = 0.4$ (Fig. 5*d*).

At a constant niobium concentration in the cationic sublattice, the electrical conductivity value and the Seebeck coefficient are changed together with increasing concentrations of sulfur or tellurium in the anionic sublattice. Thus, electrical conductivity (Fig. 6) and the Seebeck coefficient (Fig. 7) are non-monotonic functions of sulfur or tellurium contents.

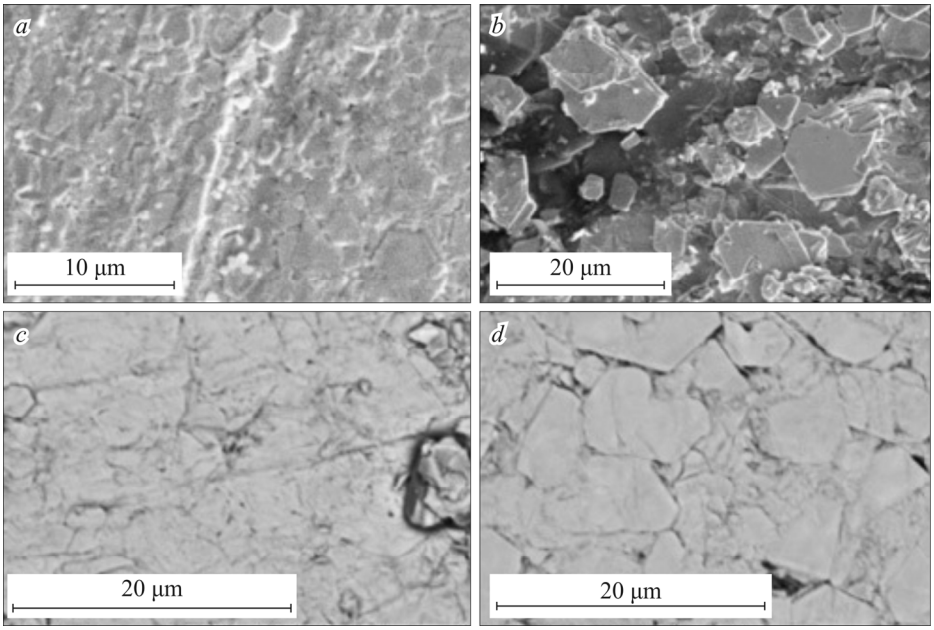

Fig. 5. SEM images of sample surfaces with compositions $W_{0.98}Nb_{0.02}Se_{1.8}S_{0.2}$ (*a*), $W_{0.98}Nb_{0.02}Se_{1.6}S_{0.4}$ (*b*), $W_{0.98}Nb_{0.02}Se_{1.8}Te_{0.2}$ (*c*), $W_{0.98}Nb_{0.02}Se_{1.6}Te_{0.4}$ (*d*).

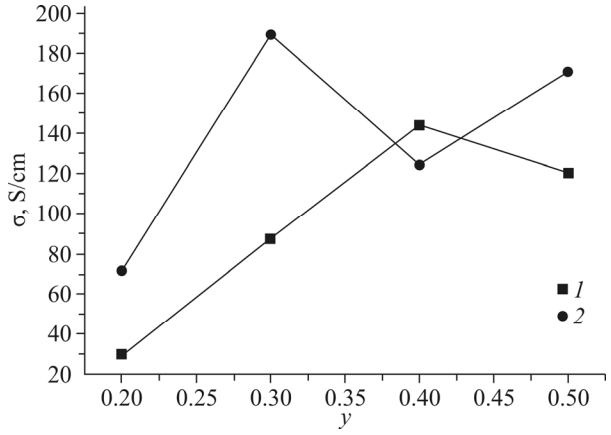

Fig. 6. Electrical conductivity at room temperature as a function of the substituting element concentration in the anionic sublattice: Te (*1*), S (*2*).

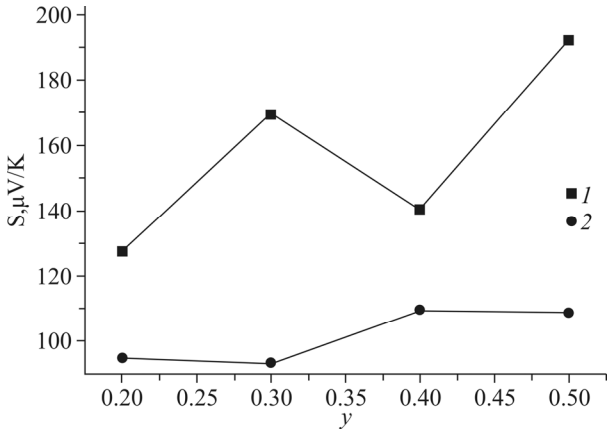

Fig. 7. The Seebeck coefficient at room temperature as a function of the substituting element concentration in the anionic sublattice: Te (*1*), S (*2*).

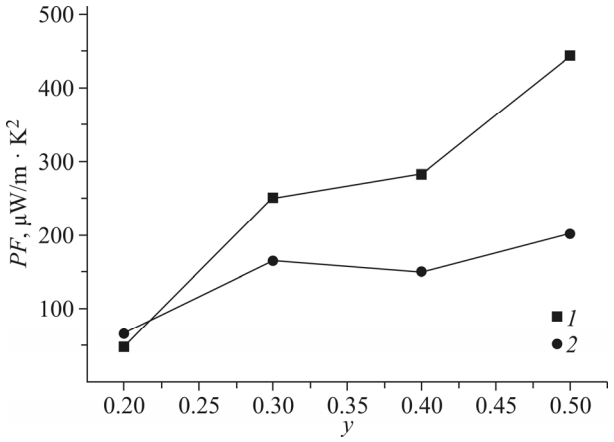

Fig. 8. Power factor *PF* at room temperature as a function of the substituting element concentration in the anionic sublattice: Te (*1*), S (*2*).

To compare the obtained changes, we calculated the power factor of studied compounds. The calculation results are shown in Fig. 8. Substitutional solid solutions with additional tellurium in the anionic sublattice demonstrate a higher thermoelectric efficiency than the samples with additional sulfur. The $W_{0.98}Nb_{0.02}Se_{1.5}Te_{0.5}$ sample has the highest *PF* value of 444.4 μW/m·K^2.

CONCLUSIONS

Varying crystallite sizes in a polycrystalline material is one possible approach to enhance thermoelectric efficiency. The crystallite sizes in substitutional solid solutions based on tungsten diselenide can be changed using substitutions in the anionic sublattice. Substitutions both by sulfur and by tellurium led to an increase in the crystallite sizes from 3 μm in pure WSe_2 to 10 μm and more in substitutional solid solutions. In the $W_{0.98}Nb_{0.02}Se_{2-y}Q_y$ (y = 0.2, 0.3, 0.4, 0.5; Q = Te, S) series, electrical conductivity and the Seebeck coefficient increased non-monotonically at room temperature with increasing sulfur or tellurium concentrations. The thermoelectric power factor *PF* also increased as a result of such changes. The sample series with additional tellurium demonstrates higher thermoelectric efficiency than the series with additional sulfur atoms. Among all samples studied at room temperature, $W_{0.98}Nb_{0.02}Se_{1.5}Te_{0.5}$ has the highest *PF* value of 444.4 μW/m·K^2.

CONFLICT OF INTERESTS

The authors declare that they have no conflict of interests.

REFERENCES

1. C. Gayner and K. K. Kar. *Prog. Mater. Sci.*, **2016**, *83*, 330.
2. K. Peng, H. Wu, Y. Yan, L. Guo, G. Wang, X. Lu, and X. Zhou. *J. Mater. Chem. A*, **2017**, *5*, 14053.
3. H. Chi, W. Liu, K. Sun, X. Su, G. Wang, P. Lostak, V. Kucek, C. Drasar, and C. Uher. *Phys. Rev. B*, **2013**, *88*, 045202.
4. Z. Zeng, P. Yang, and Z. Hu. *Appl. Surf. Sci.*, **2013**, *268*, 472.
5. K. H. Lee, W. H. Shin, H.-S. Kim, K. Lee, J. W. Roh, J. Yoo, J.-i. Kim, S. W. Kim, and S.-i. Kim. *Scr. Mater.*, **2019**, *160*, 15.
6. X. Devaux, F. Brochin, A. Dauscher, B. Lenoir, R. Martin-Lopez, H. Scherrer, and S. Scherrer. *Proc. – ICT*, **1997**, 199.
7. H. Wang, H. Yuan, S. S. Hong, Y. Li, and Y. Cui. *Chem. Soc. Rev.*, **2015**, *44*(9), 2664.
8. L. A. Chernozatonskii and A. A. Artyukh. *Phys. – Usp.*, **2018**, *61*, 2.
9. H. Imai, Y. Shimakawa, and Y. Kubo. *Phys. Rev. B*, **2001**, *64*, 241104.
10. V. L. Kalikhman and Ya. S. Umanskii. *Phys. – Usp.*, **1973**, *15*, 728.
11. A. I. Romanenko, G. E. Yakovleva, V. E. Fedorov, A. Yu. Ledneva, V. A. Kuznetsov, A. V. Sotnikov, A. R. Tsygankova, and B. M. Kuchumov. *J. Struct. Chem*., **2017**, *58* (*5*), 893.
12. G. E. Yakovleva, A. I. Romanenko, A. Yu. Ledneva, V. A. Belyavin, V. A. Kuznetsov, A. S. Berdinsky, A. T. Burkov, P. P. Konstantinov, S. V. Novikov, M.-K. Han, S.-J. Kim, and V. E. Fedorov. *J. Am. Ceram. Soc.*, **2019**, *102*, 6060.
13. W. Zhao, Z. Chorannevis, K. K. Amara, J. R. Pang, M. Toh, X. Zhang, C. Kloc, P. H. Tan, and G. Eda. *Nanoscale*, **2013**, *5*, 9677.
14. X. Duan, C. Wang, Z. Fan, G. Hao, L. Kou, U. Halim, H. Li, X. Wu, Y. Wang, J. Jiang, A. Pan, Y. Huang, R. Yu, and X. Duan. *Nano Lett.*, **2016**, *16*, 264.
15. P. Yu, J. Lin, L. Sun, Q. L. Le, X. Yu, G. Gao, C.-H. Hsu, D. Wu, T.-R. Chang, Q. Zeng, F. Liu, Q. J. Wang, H.-T. Jeng, H. Lin, A. Trampert, Z. Shen, K. Suenaga, and Z. Liu. *Adv. Mater*, **2017**, *29*, 1603991.
16. S. M. Oliver, J. Young, S. Krylyuk, T. L. Reinecke, A. V. Davydov, and P. M. Vora. *Commun. Phys.*, **2020**, *3*, 1.
17. G. E. Yakovleva, A. I. Romanenko, A. S. Berdinsky, V. A. Kuznetsov, A. Yu. Ledneva, S. B. Artemkina, and V. E. Fedorov. *Semiconductors*, **2017**, *51*, 725.
18. G. E. Yakovleva, A. I. Romanenko, A. S. Berdinsky, V. A. Kuznetsov, A. Yu. Ledneva, and V. E. Fedorov. *J. Sib. Fed. Univ*., *Math. Phys.*, **2018**, *11*, 459.